IMAGING METHODOLOGY – Mini-Review

Magnetic Resonance in Medicine 75:82–87 (2016)

Conventions and Nomenclature for Double Diffusion Encoding NMR and MRI

Noam Shemesh,[1*†] Sune N. Jespersen,[2,3†] Daniel C. Alexander,[4] Yoram Cohen,[5,6] Ivana Drobnjak,[4] Tim B. Dyrby,[7] Jurgen Finsterbusch,[8,9] Martin A. Koch,[10] Tristan Kuder,[11] Fredrik Laun,[11] Marco Lawrenz,[8] Henrik Lundell,[7] Partha P. Mitra,[12] Markus Nilsson,[13] Evren Özarslan,[14] Daniel Topgaard,[15] and Carl-Fredrik Westin[16]

Stejskal and Tanner's ingenious pulsed field gradient design from 1965 has made diffusion NMR and MRI the mainstay of most studies seeking to resolve microstructural information in porous systems in general and biological systems in particular. Methods extending beyond Stejskal and Tanner's design, such as double diffusion encoding (DDE) NMR and MRI, may provide novel quantifiable metrics that are less easily inferred from conventional diffusion acquisitions. Despite the growing interest on the topic, the terminology for the pulse sequences, their parameters, and the metrics that can be derived from them remains inconsistent and disparate among groups active in DDE. Here, we present a consensus of those groups on terminology for DDE sequences and associated concepts. Furthermore, the regimes in which DDE metrics appear to provide microstructural information that cannot be achieved using more conventional counterparts (in a model-free fashion) are elucidated. We highlight in particular DDE's potential for determining microscopic diffusion anisotropy and microscopic fractional anisotropy, which offer metrics of microscopic features independent of orientation dispersion and thus provide information complementary to the standard, macroscopic, fractional anisotropy conventionally obtained by diffusion MR. Finally, we discuss future vistas and perspectives for DDE. **Magn Reson Med 75:82–87, 2016. © 2015 Wiley Periodicals, Inc.**

Key words: double diffusion encoding; double wave vector; double pfg; microstructure; diffusion; diffusion mri

INTRODUCTION

Diffusion NMR and MRI pulse sequences extending beyond the basic Stejskal-Tanner design (1) have garnered increasing interest in recent years. Numerous modifications to the gradient waveforms have been proposed, mainly aiming to resolve novel microstructural information that could not be so easily inferred from the more conventional counterparts (2–6). One interesting modification of the waveform involves employing multiple pulsed field gradients (PFGs), and in particular, two pairs of diffusion-sensitizing gradients [for reviews, see Shemesh et al. (7), Finsterbusch (8), and Callaghan (9)]. Such sequences share a common feature: they interrogate spin displacement correlations across at least two diffusion periods to quantify microscopic properties affecting the spin's motion, such as the presence of restricting boundaries. However, as the interest in the field grows and new researchers are inspired to join this exciting endeavor, they are faced with discrepancies in the literature arising from the plethora of sequence-related naming conventions, and equally incongruent terminologies for the metrics derived from them. Some confusion also remains over what genuinely new information this kind of sequence provides, and under which circumstances it can be obtained.

Hence, the aims of the present work, which is undersigned by the vast majority of groups currently active in this field of research, were 1) to clarify existing jargon and suggest consistent terminology and naming conventions and 2) to clarify the regimes and scenarios in which genuinely novel microstructural information is accessible beyond Stejskal-Tanner sequences.

MULTIPLE DIFFUSION ENCODING NOMENCLATURE

The first basic multiple PFG pulse sequence aimed at characterizing a porous system's microstructure (in this

[1]Champalimaud Neuroscience Programme, Champalimaud Centre for the Unknown, Lisbon, Portugal.
[2]CFIN/MindLab, Aarhus University, Aarhus, Denmark.
[3]Department of Physics and Astronomy, Aarhus University, Aarhus, Denmark.
[4]Centre for Medical Image Computing, Department of Computer Science, University College London, London, United Kingdom.
[5]School of Chemistry, the Raymond and Beverly Sackler Faculty of Exact Sciences, Tel Aviv University, Tel Aviv, Israel.
[6]Sagol School of Neurosciences, Tel Aviv University, Tel Aviv, Israel.
[7]Danish Research Centre for Magnetic Resonance, Centre for Functional and Diagnostic Imaging and Research, Copenhagen University Hospital Hvidovre, Hvidovre, Denmark.
[8]Department of Systems Neuroscience, University Medical Center Hamburg-Eppendorf, Hamburg, Germany.
[9]Neuroimage Nord, University Medical Centers Hamburg–Kiel–Lübeck, Germany.
[10]Institute of Medical Engineering, University of Lübeck, Lübeck, Germany.
[11]Medical Physics in Radiology, German Cancer Research Center, Im Neuenheimer Feld 280, Heidelberg, Germany.
[12]Cold Spring Harbor Laboratory, Cold Spring Harbor, New York, USA.
[13]Lund University Bioimaging Center, Lund University, Lund, Sweden.
[14]Department of Physics, Boğaziçi University, Bebek, Istanbul, Turkey.
[15]Division of Physical Chemistry, Department of Chemistry, Lund University, Lund, Sweden.
[16]Department of Radiology, Brigham and Women's Hospital, Harvard Medical School, Boston, Massachusetts, USA.
*Correspondence to: Noam Shemesh, Ph.D., Champalimaud Neuroscience Programme, Champalimaud Centre for the Unknown, Av. Brasilia 1400-038, Lisbon, Portugal. E-mail: noam.shemesh@neuro.fchampalimaud.org
†These authors contributed equally to this work.

Received 2 April 2015; revised 13 July 2015; accepted 29 July 2015
DOI 10.1002/mrm.25901
Published online 29 September 2015 in Wiley Online Library (wileyonlinelibrary.com).

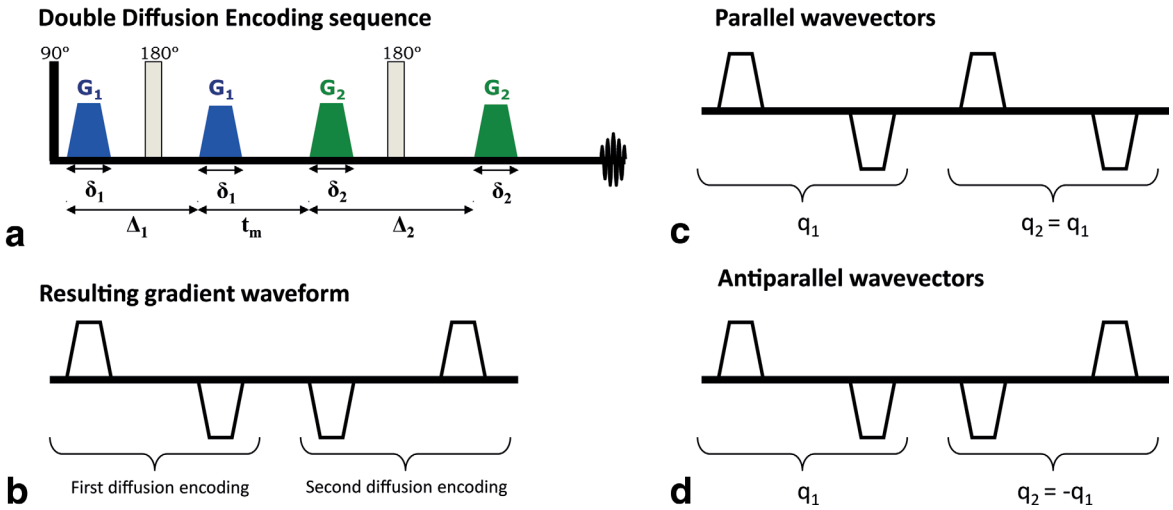

FIG. 1. (**a**) Example of a DDE sequence within the framework of a double spin echo. (**b**) The resulting gradient waveform. (**c**, **d**) Consistent definitions of parallel and antiparallel wave vectors; note that this is opposite to most previous DDE terminology.

particular case, the shape and dimensions of yeast cells) was suggested by Cory et al. (10,11) and Callaghan et al. (12,13) in the early 1990s and was generalized by Mitra (14). The sequence consists of a repeated Stejskal-Tanner design (ie, two successive diffusion-sensitizing gradient pairs) separated by a delay (mixing time), as illustrated in Figure 1. The mixing time (Fig. 1a and 1b) plays an integral part in such sequences, as it introduces another temporal variable for probing the specimen. Mixing times can be zero, resulting in temporally superimposed gradients (not shown), or finite, with the innermost gradients separated (15). In general, the pulse sequence parameters characterizing each Stejskal-Tanner block are independent, but most studies so far have used identical diffusion times and identical diffusion wave vector magnitudes $|\mathbf{q}|$ in each block [but see Åslund et al. (16), Lasič et al. (17), and Sønderby et al. (18)]. We therefore restrict our attention to this case and consider only the design shown in Figure 1b, as the particular sequence (spin echo, double spin echo, stimulated echo, and so forth) upon which it is overlaid is not conceptually critical.

This sequence has been referred to in the literature by a variety of acronyms, mainly as multiple wave vector (14) or multiple PFG, double wave vector (DWV) (19), N-PFG (20), or double PFG (dPFG or d-PFG) (15). Other names derive from the relaxation mode of the sequence, including double PGSE (21) for spin echoes and double PGSTE (22) for stimulated echoes. However, these names do not reflect inherently different experiments; rather, they refer to a sequence containing two separate diffusion encodings. The previous naming conventions all lack accuracy and/or succinctness: relaxation modes, for example, can be mixed and naming the sequences according to them may become cumbersome (eg, dPGSESTESE for an SE-STE-SE sequence). Counting the number of PFGs (as in the acronym dPFG) may also be somewhat misleading, as there are typically four rather than two PFGs in the simplest version, and the number of PFGs doubles when bipolar sequences are considered for attenuating cross-terms associated with internal gradients (22). The DWV terminology can be more accurate when gradient durations are kept short, but the concept of an effective wave vector is less useful when PFGs are long.

Because the main aim of the type of sequences shown in Figure 1 is to produce two consecutive diffusion encodings, we propose to standardize the name of this experiment class with the term double diffusion encoding (DDE). This terminology clearly identifies the primary goal of this family of sequences—to achieve two diffusion encodings—while avoiding the confusing factors listed above. Thus, the names DWV and dPFG, which have been favored by the community in recent years, are both DDE experiments. Sequences with more than two diffusion-sensitizing periods could be termed via a similar convention [eg, multiple diffusion encoding (MDE), triple diffusion encoding, and so forth]. With this convention, the Stejskal-Tanner sequence is a single diffusion encoding (SDE) sequence. If multiple DDE concatenations are used to enhance the amplitude modulation (23), the experiment should be considered as DDE because it still aims at correlating spin positions by manipulating the two principal wave vectors. Finally, a particular set of experiments where the angle ψ between the two wave vectors is varied (previously known as angular dPFG, angular dPGSE, or angular DWV), should simply be termed angular DDE.

DEFINING "PARALLEL" AND "ANTI-PARALLEL" ORIENTATIONS IN DDE

The terms "parallel" and "anti-parallel" in reference to the relative orientation of DDE's gradient wave vectors have been widely used in the past [eg, see Shemesh et al. (7) and Finsterbusch (8) and references within]. Most previous usage appears to have defined "parallel" and "anti-parallel" wave vectors by referring to the directions of the innermost gradient lobes. This presumably dates back to the simultaneous consideration of different refocusing pulse configurations in earlier papers (14). Clearly, however, each wave vector should be defined exactly in terms of the effective gradient waveform

(24,25), as shown in Figure 1b; these definitions require accounting for potential flipping effects of refocusing (π) or storage ($\pi/2$) RF pulses, as this gives the simplest and most transparent way to determine the spin phase. Following conventional notation, each wave vector should be simply defined as

$$\boldsymbol{q_i} = \frac{1}{2\pi}\gamma\delta_i \boldsymbol{G_i},$$

where γ is the gyromagnetic ratio, δ_i is the durations of the gradients in the i^{th} pulse pair, and $\boldsymbol{G_i}$ is the effective gradient corresponding to the first lobe of the ith gradient pair. For a particle located at position $\boldsymbol{r}$, $\boldsymbol{G_i}$ imparts a phase offset $e^{-i2\pi \boldsymbol{q_i}\cdot\boldsymbol{r}}$. Figures 1c and 1d illustrate this convention through examples of a more consistent definition for parallel and anti-parallel gradient orientations. Note that our current definition is opposite that of the previous usage, an issue that appears to have been overlooked in the literature.

UNIQUE MICROSTRUCTURAL INFORMATION OBTAINABLE FROM DDE AND MDE APPROACHES

Having set the naming conventions for DDE sequences and their parameters, we now discuss the unique information these experiments provide and our recommendations for its definition and terminology. We further include some comments on future focus.

Angular DDE in the zero mixing time limit has been proposed for extracting pore sizes (14), with exact solutions (15,23,26–29) as well as simulations (23,28,30) subsequently developed for this experiment in various regimes. Extensive experimental work has since explored angular DDE's potential to reconstruct pore sizes in myriad systems (19,26,31–35), and the methodology's application in vivo in humans using clinical scanners has been reported more recently (36–38). The main premise of such experiments was that they could quantify small compartment dimensions with relatively weak gradient amplitudes and that they could advantageously disambiguate the cases of restricted diffusion and multicomponent free (Gaussian) diffusion (14). Later on, these attributes were shown (39–41) to rest on the time dependence of the diffusion tensor obtainable from traditional SDE experiments. Indeed, at equally low diffusion weighting (41), one can in principle obtain the same information obtained from DDE from three individual measurements of the time-dependent diffusion tensor using SDE. Therefore, to leading order in diffusion weighting (q^2)—that is, for low diffusion weightings $2\pi qL \ll 1$, where L is the characteristic length scale—the information arising from a DDE experiment for any mixing time is in fact equivalent to the information that can be obtained from a combination of several SDE experiments (39). It remains to be determined which sequence performs better experimentally and how these microstructural measures would correspond to the actual underlying microstructure with its heterogeneity and complexity. Early evidence from simulations suggests potential practical advantages of DDE over SDE when using model-based approaches for estimating microscopic anisotropy (42).

Advantages of the DDE experiment over SDE become apparent at higher diffusion weightings for both mixing time regimes. A notable example is the emergence of zero-crossings in DDE diffraction patterns (20,43) in the short mixing time regime, which can characterize pore sizes in heterogeneous porous systems (44).

DDE experiments could also prove advantageous in studying systems characterized by orientation dispersion. To probe such a system's underlying pore dimensions and anisotropy (45–49) with SDE, model-based approaches are generally necessary. On the other hand, theory has shown that angular DDE can distinguish a population of spherical pores from a macroscopically isotropic system of anisotropic pores and quantify underlying microstructural features such as pore dimensions and anisotropy without imposing modeling constraints (10,14). Later work generalized this theory (50–52) and validated it through a wide range of experiments in heterogeneous systems, including phantoms (44,53), isolated gray matter (54) and whole brain tissues (50), and in vivo experiments in rodents (55) and humans on clinical scanners (37). The latter works showed intriguing new contrasts in brain tissue.

TERMINOLOGY FOR DDE- (OR MDE)-DERIVED METRICS

Studies to date have used a variety of different indices to quantify pore anisotropy and have adopted many different names for those indices, including compartment shape anisotropy (52), pore shape anisotropy (39), compartment shape eccentricity (50), (apparent) compartment eccentricity (55), and microscopic anisotropy (21,51). Importantly, for arbitrary diffusion times (52), in a population of identical pores, the measurable part of the angular DDE signal responsible for the contrast between spherical and anisotropic pores (q^4 term) reflects the underlying diffusion anisotropy within a single pore in the ensemble (50). In fact, it is directly proportional to the variance of the eigenvalues σ_i of the pore's diffusion tensor (50) (ie, the effective diffusion tensor of spins in the pore). We therefore propose the term microscopic diffusion anisotropy (μA), because it is a microscopic property affecting diffusion that is independent of both reference frame and pore orientation distribution. Hence,

$$\begin{aligned} &\mu\mathrm{A}^2 \propto (\sigma_1-\bar{\sigma})^2+(\sigma_2-\bar{\sigma})^2+(\sigma_3-\bar{\sigma})^2, \\ &\bar{\sigma} = (\sigma_1+\sigma_2+\sigma_3)/3. \end{aligned} \quad [1]$$

μA is a time-dependent property; if diffusion times are too short to probe the boundaries, it will vanish, whereas in the opposite limit of a long diffusion time, it will reflect compartment eccentricity. However, as evident from Equation 1, μA will also depend on compartment size, which affects the diffusion tensor magnitude. The term "microscopic anisotropy" was used previously to describe local anisotropy of the diffusion propagator in the vicinity of macroscopic boundaries (56), but the current proposal is more akin to Callaghan and Komlosh's local diffusion anisotropy (57), which reflects properties of the propagator averaged over the compartment.

Normalized versions of μA (50,58,59) aim to remove the dependence on compartment size. In analogy to FA (60), microscopic fractional anisotropy (μFA) normalizes μA by dividing it by a measure of the size of the diffusion tensor (50,58–60):

$$\mu\mathrm{FA} = \sqrt{\frac{3}{2}\frac{(\sigma_1 - \bar{\sigma})^2 + (\sigma_2 - \bar{\sigma})^2 + (\sigma_3 - \bar{\sigma})^2}{\sigma_1^2 + \sigma_2^2 + \sigma_3^2}}. \quad [2]$$

For populations of coherently aligned pores (ie, no orientation dispersion), μFA and FA are in fact identical (50,58,59). Dispersion in the orientation of the pores affects FA, but not μFA, because the pore's microscopic environment is independent of orientation. Therefore, DDE experiments can disentangle two distinct factors influencing the FA, namely local compartment eccentricity and orientation dispersion. Rotationally invariant designs of DDE measurements are now available (37,50,51,61) to extract μFA in the absence of knowledge about specific symmetries (32,33). On the other hand, rotationally variant measurements [eg, DDE experiments in a single plane (32,33)] will generally make the μFA depend on experimental parameters, and in such cases we suggest that the extractable parameter could be preceded by an "apparent" qualifier. Unnormalized versions of microscopic diffusion anisotropy (50,51,62) can sometimes be advantageous, as they are additive over pore types and therefore reflect the population weighted average of the microscopic diffusion anisotropy when distinct pore types are present. This is in contrast to μFA, which combines μFA from different pore type populations in a nonlinear fashion.

We would like to point out here that μFA probably cannot be derived from conventional SDE experiments without imposing modeling assumptions, and thus it appears to be a hallmark of the MDE class of experiments with the angular DDE version being quite efficient in extracting the sought-after microstructural information.

PERSPECTIVES AND FUTURE OUTLOOK FOR DDE-MRI

It is clear that DDE can provide new ways of looking into the brain and other tissues in vivo. DTI-like metrics (eg, FA, eigenvalues) can be derived directly from rotationally invariant DDE designs (50). Such designs have acquisition requirements similar to those for a typical 60-direction DTI experiment. As μFA and FA provide complementary information about the local microstructure and the more macroscopic ensemble orientation, and because both metrics can be obtained from the same DDE experiment, this approach could be highly fruitful, leading to a richer description of the brain's microstructure, especially in the gray matter and other orientationally dispersed systems. Other gradient waveforms/schemes to evaluate μFA have been employed recently (58,63–66), and it will be highly interesting from a methodological perspective to compare μFAs across the different schemes. The time dependence of μA and μFA could also lead to further insights into tissue microarchitecture. Another vista worth mentioning is the measurement of such metrics for metabolic signals in vivo (67), as the increased cellular specificity may prove highly advantageous in understanding the biophysical origins of μFA and how they are altered upon disease.

Finally, it is worth noting the distinction between diffraction patterns from DDE and SDE; the former 1) remain preserved upon heterogeneity (20,44) and 2) may preserve phase information (20,68–70), enhancing the possibility that pore microstructures could potentially be imaged exactly. In addition, the resolution of size distributions by measuring DDE diffraction patterns as function of relative diffusion wave vector angle appear promising (71). These and related measures extracted from MDE experiments are important for the emerging field of in vivo virtual histology by providing microstructural parameters that could potentially distinguish different pathological brain states in new ways that are different from the more familiar forms arising from conventional SDE. The biomedical implications of impaired brain microstructure provide a strong impetus for deepening our study of the subject outlined in this work. All these highly exciting avenues are currently being explored, and we trust that this mini-review will help to encourage both preclinical and clinical communities to explore the immense potential of DDE experiments.

ACKNOWLEDGMENTS

We are grateful to the Marcus Wallenberg Foundation for the International Scientific Collaboration and CR Development AB for sponsoring the Double PFG Workshop 2013 in Jukkasjärvi, Sweden.

REFERENCES

1. Stejskal EO, Tanner JE. Spin diffusion measurements: spin echoes in the presence of a time-dependent field gradient. J Chem Phys 1965; 42:288–292.
2. Laun FB, Kuder TA. Diffusion pore imaging with generalized temporal gradient profiles. Magn Reson Imaging 2013;31:1236–1244.
3. Drobnjak I, Siow B, Alexander DC. Optimizing gradient waveforms for microstructure sensitivity in diffusion-weighted MR. J Magn Reson 2010;206:41–51.
4. Kiruluta AJ. Probing restrictive diffusion dynamics at short time scales. J Magn Reson 2008;192:27–36.
5. Does MD, Parsons EC, Gore JC. Oscillating gradient measurements of water diffusion in normal and globally ischemic rat brain. Magn Reson Med 2003;49:206–215.
6. Gore JC, Xu J, Colvin DC, Yankeelov TE, Parsons EC, Does MD. Characterization of tissue structure at varying length scales using temporal diffusion spectroscopy. NMR Biomed 2010;23:745–756.
7. Shemesh N, Özarslan E, Komlosh ME, Basser PJ, Cohen Y. From single-pulsed field gradient to double-pulsed field gradient MR: gleaning new microstructural information and developing new forms of contrast in MRI. NMR Biomed 2010;23:757–780.
8. Finsterbusch J. Multiple-wave-vector diffusion-weighted NMR. In: Graham AW, editor. Annual reports on NMR spectroscopy. Volume 72. Oxford, UK: Academic Press; 2011. p 225–299.
9. Callaghan PT. Translational dynamics and magnetic resonance: principles of pulsed gradient spin echo NMR. Oxford,UK: Oxford University Press; 2011. 547 p.
10. Cory DG, Garroway AN, Miller JB. Applications of spin transport as a probe of local geometry. Polym Preprints 1990;31:149.
11. Cheng Y, Cory DG. Multiple scattering by NMR. J Am Chem Soc 1999;121:7935–7936.
12. Callaghan PT, Xia Y. Velocity and diffusion imaging in dynamic NMR microscopy. J Magn Reson 1991;91:326–352.
13. Callaghan PT, Codd SL, Seymour JD. Spatial coherence phenomena arising from translational spin motion in gradient spin echo experiments. Concepts Magn Reson 1999;11:181–202.

14. Mitra PP. Multiple wave-vector extensions of the NMR pulsed-field-gradient spin-echo diffusion measurement. Phys Rev B Condens Matter 1995;51:15074–15078.
15. Özarslan E, Basser PJ. Microscopic anisotropy revealed by NMR double pulsed field gradient experiments with arbitrary timing parameters. J Chem Phys 2008;128:154511.
16. Åslund I, Nowacka A, Nilsson M, Topgaard D. Filter-exchange PGSE NMR determination of cell membrane permeability. J Magn Reson 2009;200:291–295.
17. Lasič S, Nilsson M, Latt J, Stahlberg F, Topgaard D. Apparent exchange rate mapping with diffusion MRI. Magn Reson Med 2011; 66:356–365.
18. Sønderby CK, Lundell HM, Søgaard LV, Dyrby TB. Apparent exchange rate imaging in anisotropic systems. Magn Reson Med 2014;72:756–762.
19. Koch MA, Finsterbusch J. Compartment size estimation with double wave vector diffusion-weighted imaging. Magn Reson Med 2008;60: 90–101.
20. Özarslan E, Basser PJ. MR diffusion—"diffraction" phenomenon in multi-pulse-field-gradient experiments. J Magn Reson 2007;188:285–294.
21. Komlosh ME, Horkay F, Freidlin RZ, Nevo U, Assaf Y, Basser PJ. Detection of microscopic anisotropy in gray matter and in a novel tissue phantom using double pulsed gradient spin echo MR. J Magn Reson 2007;189:38–45.
22. Shemesh N, Cohen Y. Overcoming apparent susceptibility-induced anisotropy (aSIA) by bipolar double-pulsed-field-gradient NMR. J Magn Reson 2011;212:362–369.
23. Finsterbusch J. Extension of the double-wave-vector diffusion-weighting experiment to multiple concatenations. J Magn Reson 2009;198: 174–182.
24. Callaghan PT. Principles of nuclear magnetic resonance microscopy. Oxford, UK: Clarendon Press; 1991. 516 p.
25. Karlicek RF, Lowe IJ. Modified pulsed gradient technique for measuring diffusion in the presence of large background gradients. J Magn Reson 1980;37:75–91.
26. Shemesh N, Özarslan E, Basser PJ, Cohen Y. Measuring small compartmental dimensions with low-q angular double-PGSE NMR: the effect of experimental parameters on signal decay. J Magn Reson 2009;198:15–23.
27. Özarslan E, Shemesh N, Basser PJ. A general framework to quantify the effect of restricted diffusion on the NMR signal with applications to double pulsed field gradient NMR experiments. J Chem Phys 2009; 130:104702.
28. Finsterbusch J. Numerical simulations of short-mixing-time double-wave-vector diffusion-weighting experiments with multiple concatenations on whole-body MR systems. J Magn Reson 2010;207:274–282.
29. Jespersen SN, Buhl N. The displacement correlation tensor: microstructure, ensemble anisotropy and curving fibers. J Magn Reson 2011;208:34–43.
30. Koch MA, Finsterbusch J. Numerical simulation of double-wave vector experiments investigating diffusion in randomly oriented ellipsoidal pores. Magn Reson Med 2009;62:247–254.
31. Shemesh N, Özarslan E, Bar-Shir A, Basser PJ, Cohen Y. Observation of restricted diffusion in the presence of a free diffusion compartment: single- and double-PFG experiments. J Magn Reson 2009;200: 214–225.
32. Komlosh ME, Özarslan E, Lizak MJ, Horkay F, Schram V, Shemesh N, Cohen Y, Basser PJ. Pore diameter mapping using double pulsed-field gradient MRI and its validation using a novel glass capillary array phantom. J Magn Reson 2011;208:128–135.
33. Weber T, Ziener CH, Kampf T, Herold V, Bauer WR, Jakob PM. Measurement of apparent cell radii using a multiple wave vector diffusion experiment. Magn Reson Med 2009;61:1001–1006.
34. Özarslan E, Komlosh ME, Lizak MJ, Horkay F, Basser PJ. Double pulsed field gradient (double-PFG) MR imaging (MRI) as a means to measure the size of plant cells. Magn Reson Chem 2011;49(suppl 1): S79–S84.
35. Shemesh N, Özarslan E, Basser PJ, Cohen Y. Accurate noninvasive measurement of cell size and compartment shape anisotropy in yeast cells using double-pulsed field gradient MR. NMR Biomed 2012;25: 236–246.
36. Koch MA, Finsterbusch J. Towards compartment size estimation in vivo based on double wave vector diffusion weighting. NMR Biomed 2011;24:1422–1432.
37. Lawrenz M, Finsterbusch J. Double-wave-vector diffusion-weighted imaging reveals microscopic diffusion anisotropy in the living human brain. Magn Reson Med 2013;69:1072–1082.
38. Avram AV, Özarslan E, Sarlls JE, Basser PJ. In vivo detection of microscopic anisotropy using quadruple pulsed-field gradient (qPFG) diffusion MRI on a clinical scanner. Neuroimage 2013;64:229–239.
39. Jespersen SN. Equivalence of double and single wave vector diffusion contrast at low diffusion weighting. NMR Biomed 2012;25:813–818.
40. Jensen JH. Sufficiency of diffusion tensor in characterizing the diffusion MRI signal to leading order in diffusion weighting. NMR Biomed 2014;27:1005–1007.
41. Jespersen SN. Comment on "Measuring small compartments with relatively weak gradients by angular double-pulsed-field-gradient NMR" by Morozov Bar, Sochen, and Cohen. Magn Reson Imaging 2013;31: 1643–1644.
42. Ianuş A, Drobnjak I, Alexander DC. Model-based estimation of microscopic anisotropy in macroscopically isotropic substrates using diffusion MRI. Inf Process Med Imaging 2015;24:699–710.
43. Shemesh N, Cohen Y. The effect of experimental parameters on the signal decay in double-PGSE experiments: negative diffractions and enhancement of structural information. J Magn Reson 2008;195: 153–161.
44. Shemesh N, Özarslan E, Adiri T, Basser PJ, Cohen Y. Noninvasive bipolar double-pulsed-field-gradient NMR reveals signatures for pore size and shape in polydisperse, randomly oriented, inhomogeneous porous media. J Chem Phys 2010;133:044705.
45. Stanisz GJ, Szafer A, Wright GA, Henkelman RM. An analytical model of restricted diffusion in bovine optic nerve. Magn Reson Med 1997;37:103–111.
46. Assaf Y, Freidlin RZ, Rohde GK, Basser PJ. New modeling and experimental framework to characterize hindered and restricted water diffusion in brain white matter. Magn Reson Med 2004;52:965–978.
47. Jespersen SN, Kroenke CD, Østergaard L, Ackerman JJ, Yablonskiy DA. Modeling dendrite density from magnetic resonance diffusion measurements. Neuroimage 2007;34:1473–1486.
48. Zhang H, Schneider T, Wheeler-Kingshott CA, Alexander DC. NODDI: practical in vivo neurite orientation dispersion and density imaging of the human brain. Neuroimage 2012;61:1000–1016.
49. Panagiotaki E, Schneider T, Siow B, Hall MG, Lythgoe MF, Alexander DC. Compartment models of the diffusion MR signal in brain white matter: a taxonomy and comparison. Neuroimage 2012; 59:2241–2254.
50. Jespersen SN, Lundell H, Sønderby CK, Dyrby TB. Orientationally invariant metrics of apparent compartment eccentricity from double pulsed field gradient diffusion experiments. NMR Biomed 2013;26: 1647–1662.
51. Lawrenz M, Koch MA, Finsterbusch J. A tensor model and measures of microscopic anisotropy for double-wave-vector diffusion-weighting experiments with long mixing times. J Magn Reson 2010;202:43–56.
52. Özarslan E. Compartment shape anisotropy (CSA) revealed by double pulsed field gradient MR. J Magn Reson 2009;199:56–67.
53. Shemesh N, Adiri T, Cohen Y. Probing microscopic architecture of opaque heterogeneous systems using double-pulsed-field-gradient NMR. J Am Chem Soc 2011;133:6028–6035.
54. Shemesh N, Cohen Y. Microscopic and compartment shape anisotropies in gray and white matter revealed by angular bipolar double-PFG MR. Magn Reson Med 2011;65:1216–1227.
55. Shemesh N, Barazany D, Sadan O, Bar L, Zur Y, Barhum Y, Sochen N, Offen D, Assaf Y, Cohen Y. Mapping apparent eccentricity and residual ensemble anisotropy in the gray matter using angular double-pulsed-field-gradient MRI. Magn Reson Med 2012;68: 794–806.
56. Özarslan E, Nevo U, Basser PJ. Anisotropy induced by macroscopic boundaries: surface-normal mapping using diffusion-weighted imaging. Biophys J 2008;94:2809–2818.
57. Callaghan PT, Furo I. Diffusion-diffusion correlation and exchange as a signature for local order and dynamics. J Chem Phys 2004;120: 4032–4038.
58. Lasič S, Szczepankiewicz F, Eriksson S, Nilsson M, Topgaard D. Microanisotropy imaging: quantification of microscopic diffusion anisotropy and orientational order parameter by diffusion MRI with magic-angle spinning of the q-vector. Front Phys 2014. http://dx.doi.org/10.3389/fphy.2014.00011.
59. Jespersen SN, Lundell H, Sønderby CK, Dyrby TB. Commentary on "Microanisotropy imaging: quantification of microscopic diffusion

anisotropy and orientation of order parameter by diffusion MRI with magic-angle spinning of the q-vector." Front Phys 2014. http://dx.doi.org/10.3389/fphy.2014.00028.
60. Basser PJ, Pierpaoli C. Microstructural and physiological features of tissues elucidated by quantitative-diffusion-tensor MRI. J Magn Reson Series B 1996;111:209–219.
61. Lawrenz M, Finsterbusch J. Mapping measures of microscopic diffusion anisotropy in human brain white matter in vivo with double-wave-vector diffusion-weighted imaging. Magn Reson Med 2015;73:773–783.
62. Lawrenz M, Brassen S, Finsterbusch J. Microscopic diffusion anisotropy in the human brain: Reproducibility, normal values, and comparison with the fractional anisotropy. Neuroimage 2015;109:283–297.
63. Eriksson S, Lasič S, Topgaard D. Isotropic diffusion weighting in PGSE NMR by magic-angle spinning of the q-vector. J Magn Reson 2013;226:13–18.
64. Szczepankiewicz F, Lasič S, van Westen D, Sundgren PC, Englund E, Westin CF, Ståhlberg F, Lätt J, Topgaard D, Nilsson M. Quantification of microscopic diffusion anisotropy disentangles effects of orientation dispersion from microstructure: applications in healthy volunteers and in brain tumors. Neuroimage 2015;104:241–252.
65. Westin CF, Szczepankiewicz F, Pasternak O, Özarslan E, Topgaard D, Knutsson H, Nilsson M. Measurement tensors in diffusion MRI: generalizing the concept of diffusion encoding. Medical image computing and computer-assisted intervention: MICCAI International Conference on Medical Image Computing and Computer-Assisted Intervention 2014;17(Pt 3):209–216.
66. Jensen JH, Hui ES, Helpern JA. Double-pulsed diffusional kurtosis imaging. NMR Biomed 2014;27:363–370.
67. Shemesh N, Rosenberg JT, Dumez JN, Muniz JA, Grant SC, Frydman L. Metabolic properties in stroked rats revealed by relaxation-enhanced magnetic resonance spectroscopy at ultrahigh fields. Nat Commun 2014;5:4958.
68. Kuder TA, Laun FB. NMR-based diffusion pore imaging by double wave vector measurements. Magn Reson Med 2013;70:836–841.
69. Shemesh N, Westin CF, Cohen Y. Magnetic resonance imaging by synergistic diffusion-diffraction patterns. Phys Rev Lett 2012;108:058103.
70. Laun FB, Kuder TA, Semmler W, Stieltjes B. Determination of the defining boundary in nuclear magnetic resonance diffusion experiments. Phys Rev Lett 2011;107:048102.
71. Katz Y, Nevo U. Quantification of pore size distribution using diffusion NMR: experimental design and physical insights. J Chem Phys 2014;140:164201.